Characterization and Sensing Potential of Indium Oxide-Vanadium Oxide Thin Films for Smart Devices

Ahmed Yaseen, Ziad T. Khodair and Nadia Mohammed Jassim
Department of Physics,College of Science, University of Diyala, 32001 Baqubah, Iraq
ahmedyaseen@uodiyala.edu.iq, ziad_tariq70@yahoo.com, nadiajassim@uodiyala.edu.iq

Keywords: In_2O_3–V_2O_5 Thin Films, Pulsed Laser Deposition, Nanocomposites, XRD Analysis, FE-SEM Characterization, Optical Band Gap, Optoelectronic Applications, Photodetectors.

Abstract: In this study, the effects of indium oxide (In_2O_3) mixing in the crystal lattice structure of vanadium oxide(V_2O_5) were investigated and fabricated by a facile and cost-effective method via the Pulsed Laser Deposition (PLD) technique using the following constant parameters: energy (280 mJ/pulse), frequency (1 Hz), number of pulses (700 pulses), and the angle of incidence was 45° with 1064 nm laser wavelengths, 100°C temperature substrate and annealing temperature (400°C). X-ray diffraction (XRD) analysis revealed the formation of a cubic phase for In_2O_3. Since the intensity of the phase and angle 2θ match the Miller indices, the thin film's structure will be more crystalline at a laser wavelength of 1064 nm. And an orthorhombic phase for V_2O_5. It was observed that the lattice parameters of the composite sample were decreased compared with the pure In_2O_3, but the crystallite sizes of sample V_2O_5 80% were increased as a result of the substitution of vanadium in the crystal lattice of In_2O_3. The morphological characteristics of the Field Emission Scanning Electron Microscopy (FE-SEM) showed that all samples have spherical shapes, and their distribution sizes are between 31.7nm for In_2O_3, 208.3 nm for V_2O_5, and 176.6nm for V_2O_5 80% ratio and thickness 280.2nm,651nm,301nm respectively. It was found that the average sizes of nanoparticles decreased due to the presence of an amount of indium oxide. To characterize the optical characteristics (UV-vis) spectra, a decrease was found in the band gap(2.83ev) of the In_2O_3 20% -V_2O_5 80% sample compared with energy gap(3.31ev) of pure In_2O_3.

1 INTRODUCTION

The efficiency and adaptability of transition metal oxides in sensors, memory, solar cells, security, surveillance, and healthcare are drawing interest in the production of electronic devices. This is mostly because of their exceptional optical and electrical characteristics, as well as their capacity to go through reversible phase transitions between semiconductor and metallic states, among the oxides of vanadium. Vanadium pentoxide (V_2O_5) stands out as a particularly attractive option due to its exceptional chemical and electronic properties that distinguish it from its competitors. Numerous reports have highlighted its use in the development of field-effect transistors, demonstrating the range of applications in which its potential is being realized. Electronic technologies that adopt V_2O_5 may see revolutionary improvements in functionality and performance [1]. In optoelectronic applications like photodetectors, V_2O_5 is a perfect choice due to its direct band gap of 2.61eV [2].Recent studies have reported synthesizing various V_2O_5 structures, including nanowires, nanotubes, and nano spheres, for use in photodetectors made with various methods [3], [4].

Despite reports of V_2O_5 one-dimensional (1D) structures, the material's small surface area restricts charge transport and makes it difficult to define contacts on 1D structures. A highly exposed area is a natural advantage of two-dimensional(2D) structures, and making electrical connections on 2D structures is not too difficult because of its propensity to be present in various oxidation states, it is hard to define contacts on V_2O_5 one-dimensional (1D) structures because of the material's small surface area, which restricts charge transport. Two-dimensional (2D) structures naturally have a significantly exposed surface, and creating electrical connections on 2D structures is not too difficult due to their tendency to be present in different oxidation states. Deposition and growth of the vanadium oxide phases are not easy. VO_2 or V_2O_5 growth requires management of the synthesis

parameters. There are numerous methods for producing metal oxides, including sol-gel, hydrothermal, electrospinning, and sputtering [5], [6]. Other methods of deposition include physical vapor deposition, which is inefficient in terms of both time and energy. The benefit of hydrothermal synthesis over these techniques is that, by adjusting variables like temperature and time, the morphology and oxidation states can be controlled. Because flexible resistive memories have so many potentials uses in the fields of neuromorphic computing, analog electronics, and artificial intelligence, they have become very popular A wide bandgap semiconductor with dielectric qualities is 2D V_2O_5. Thereby making it suitable for resistive memory applications. The integration of a 2D V_2O_5 layered structure [7].

Furthermore, doping In_2O_3 with V_2O_5 causes a red transfer in the energy gap, which raises the transmittance of infrared light. Transparent conductors were the ideal application for IVO films made with different concentrations [8], reaching a coefficient of 4.35×10^{-3} ohm^{-1}. They ascribed this improvement to the shift in the band caused by the approach between the conduction band's minimum and the Fermi level [9], that the doping of indium oxide (InO_3:V) thin film with V at a concentration of 50 nm improved the transmittance to approximately 86 percent in the near infrared range. while ZnO film doped with vanadium at greater concentrations reduced light transmission [9], [10]. However, ITO films don't absorb well in the near-infrared spectrum. Our objective in this study was to combine In_2O_3 and V_2O_5 to increase the transmittance of near-infrared light, which would increase the efficiency of the photodetector.

2 MANUSCRIPT PREPARATION

2.1 Materials and Methodology

A sample of (In_2O_3) with a purity of 99.99% from CDH, and a sample of (V_2O_5) with a purity of 99.5% from CDH in England.The powders were mixed in specific weight ratios using mechanical (manual) mixing according to the Table 1 below.

After preparing the target which is made of pure materials (In_2O_3) and (V_2O_5), the thin films deposition process is initiated by PLD. Thin-film deposition required a 45-minute cleaning of the glass, using an ultrasonic bath with distilled water (15 minutes), ethanol (15 minutes), and distilled water again (15 minutes). The synthesized technique is used a pulsed Nd: YAG laser with the following specifications wavelength λ = 1064 nm, energy 280 mJ/pulse, frequency 1 Hz, and pressure 1 mbar. The target was 4 cm from the substrate, the substrate temperature was 100 °C, the number of pulses was 700pulse, and the angle of incidence was 45°. To improve crystallization and reduce crystal defects, thereby enhancing the electrical and optical properties of the films, the prepared films were annealed at 400 °C for three hours.

Table 1: The weight ratios for preparing the samples.

Samples	Weight of ratio	Pressing	Diameter of mold	Sintering
In_2O_3	1.5 g	100 bar	12 mm	400c° for 3hr
V_2O_5	1.5 g			
In_2O_3 20%-V_2O_5 80%	0.424-1.113 g			

3 RESULTS AND DISCUSSION

3.1 X-ray Diffraction of the In2O3, V2O5 and In2O3 - V2O5 Thin Films Deposited by PLD

The X-ray diffraction results of nanostructured indium oxide thin films deposited on a glass substrate are shown in Figure 1. The diffraction pattern of pure indium oxide exhibits the highest intensity peaks at 2θ angles of 30.62°, 35.49°, 51.05°, 21.53°, and 60.69°. These peaks correspond to the (222), (400), (440), (211), and (622) crystallographic planes, respectively. The presence of these reflections confirms that the films possess a polycrystalline cubic structure consistent with the ICDD reference card (JCPDS 01-071-2194).

The crystallite size was determined using the standard Scherrer approach [11], which relates the size to the wavelength of X-rays, the peak broadening, and the diffraction angle. The analysis yielded an average crystallite size of 43.58 nm, while the lattice constant was found to be approximately 9.6 Å.

Under the applied deposition and annealing conditions, the typical crystallite size for pulsed laser deposited indium oxide thin films ranges from 41.25 to 53.13 nm, which is in good agreement with the obtained results.

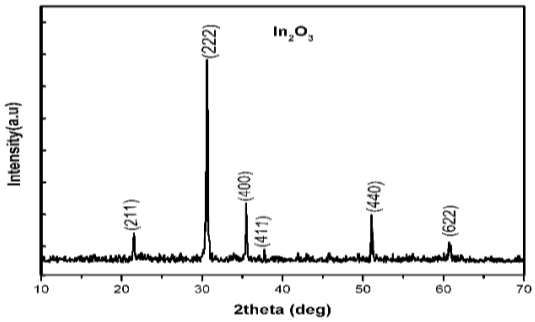

Figure 1: The XRD patterns of the In2O3 thin films deposited by PLD.

Figure 2 shows of X-ray diffraction (XRD) patterns of V_2O_5 films deposited using (PLD) at a pressure of 2×10^{-2} mbar, these patterns reveal a polycrystalline structure in the films deposited at temperatures as low as 100 °C. Notably, the predominant peak observed corresponds to the (010) orientation of the orthorhombic V_2O_5 phase. The polycrystalline nature of V_2O_5 this deposition temperature demonstrates one of PLD's primary benefits over alternative physical vapor deposition techniques., such as electron-beam evaporation and sputtering, which typically require deposition temperatures in the range of 300–500 °C. Which is agreement with reference [12]. A reported amorphous structure was observed at temperatures below 300 °C using the vacuum evaporation technique. The lower crystallization temperature seen in the case of Pulsed Laser Deposition (PLD) can be attributed to the high kinetic energy (>1 eV) of the ejected species from the laser-produced plasma. When these condensed particles are deposited, they carry high energies. As a result, the mobility of ad-atoms allows for the formation of highly oriented nano-crystalline films, even at low temperatures [12]. From XRD measurements, we conclude that each film has a nanocrystalline structure. The peaks are lying at approximately 2θ=20.2°, 26.15°, and 12.6°, indicating the orthorhombic V_2O_5 phase (JCPDS card no. 00-041-1426, space group: Pmnm (59), a = 11.51 Å, b = 4.369 Å, c= 3.563 Å). They are appropriate to the (010), (101), and (100) reflections, respectively [13]. The β phase is created by annealing thin films at temperatures between 370 to 600°C. It is distinguished by a layered structure with weak interlayer bonding [14]. As can be seen at angles 31.05° and 20.2°attributed to (ICSD card 00-041-1426), the thin film exhibits an initial transformation to the B-v_2O_5 phase after annealing at 400°C for 3h. This is caused by the rearrangement of oxygen atoms and the transition of v-o-v bonds [12], [15]. The calculated sizes of the partical are presented in Table 2. It is important to note that these size values represent the average crystallite size at the location where the X-ray beam passed through [16].

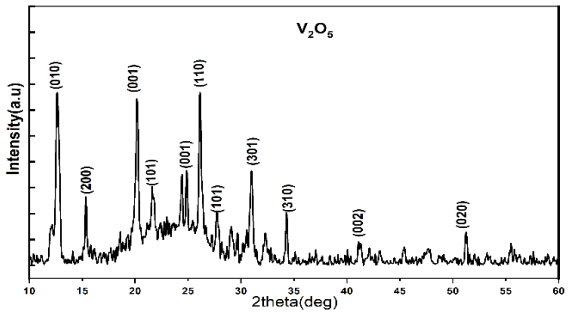

Figure 2: XRD diffraction patterns of V_2O_5 thin films.

Figure 3 shows the comparative X-ray diffraction patterns of the In_2O_3 20% and V_2O_5 80% samples. The diffraction pattern of InVO indicates the presence of both V_2O_5 and In_2O_3 phases, with their diffraction peaks corresponding to the reference PDF patterns JCPDS no. 00-041-1426 and 01-071-2194, respectively. A prominent peak is observed at 2θ = 12.59˚, related to the V_2O_5 (010) plane, indicating substantial growth along this plane. Additionally, the pattern reveals a notable increase in the diffraction intensity of V_2O_5 within InVO, indicating enhanced crystallinity. The rise in InVO crystallinity underscores In_2O_3 vital role in coating the V_2O_5 surface; this reduces grain size, which is beneficial for optical characteristics.[17].

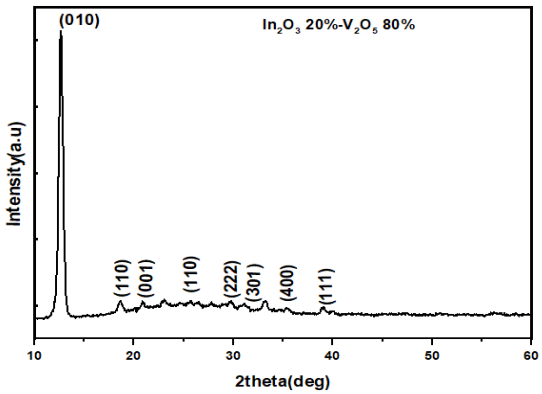

Figure:3 XRD diffraction patterns of In_2O_3 20%- V_2O_5 80%thin films.

Lastly, extremely crystalline composite V_2O_5-In_2O_3 nanocrystals with a structure were created, as evidenced by the high intensity of cubic-phase peaks

and the absence of secondary-phase peaks. The absence of vanadium oxide phases implies that most of the V ions were incorporated into the In_2O_3 host lattice. The lack of a featured peak shift upon ratio V_2O_5 80% is due to the similar ionic radii of V^{3+} ions (0.78 Å) and In^{3+} ions (0.80 Å) [18].

3.2 Structural Characterization, Field Emission Scanning Electron Microscopy (FE-SEM)

Figure 4a, b and c displays the indium oxide films' morphology was studied by FE-SEM at 500nm, 1µm and annealing of 400˚c for 3h. Images of In_2O_3 films deposited at 1064nm laser wavelengths, 280 mJ,1Hz,100˚c temperature of substrate, 700 pulses, and pressure 10^{-2} mbar, the average diameters of the In_2O_3 particles were 31.77 nm. The film reveals that it covered the glass substrate surface with uniform particles with an average diameter of 31.77 nm. and uniform surface morphology with dense homogeneous grain distribution as shown in three-dimensional by ImageJ program Figure 4c, The growing process and the combination of tiny grains caused droplets and particles with submicron sizes to be spotted across the film surface [19]-[21].

Figure 5 provides a clear example of the grain growth of the V_2O_5 films through its FE-SEM image. Figure 5 (a-200nm and b-1µm) images demonstrate that the V_2O_5 films have a microstructure with nearly spherical and nanosized grains that are evenly dispersed across the surface of the glass substrate as shown in Figure 5c, the density of particles appearing on the surface of the vanadium oxide film has a regular distribution at a temperature of 400°C for 3h. The average grain size is approximately 208.3 nm [22].

An important finding in this study is the notable transformation in surface morphology of the V_2O_5 films with increasing percentage of vanadium oxide compared to indium oxide, as illustrated in Figure 6a, b and c. These morphological changes are dominant at the ratio In_2O_3 20% -V_2O_5 80% and temperatures 400 °C for 3h. The significant affecting grain size, shape, and their overall distribution highlighting the critical nature of these conditions for optimizing film performance, with uniform particles and an average diameter of 176.61nm Which proves that the film has a high surface area due to the symmetrical distribution density of particles on the surface this effect is due to the ratio of indium oxide in the film as shown in the Figure 6c, [23], [24].

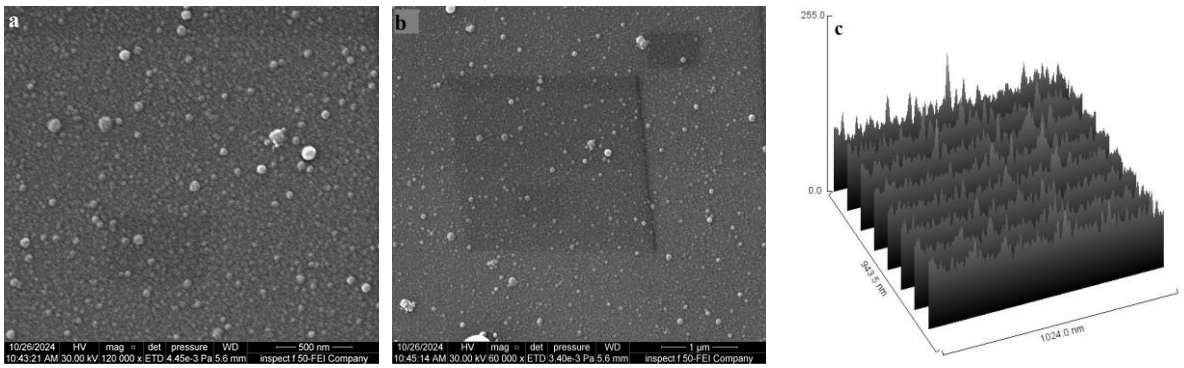

Figure 4: Micrographs of the surface of oxide materials obtained by FE-SEM thin film for In_2O_3 a) 500nm, b) 1µm, c) dense distribution.

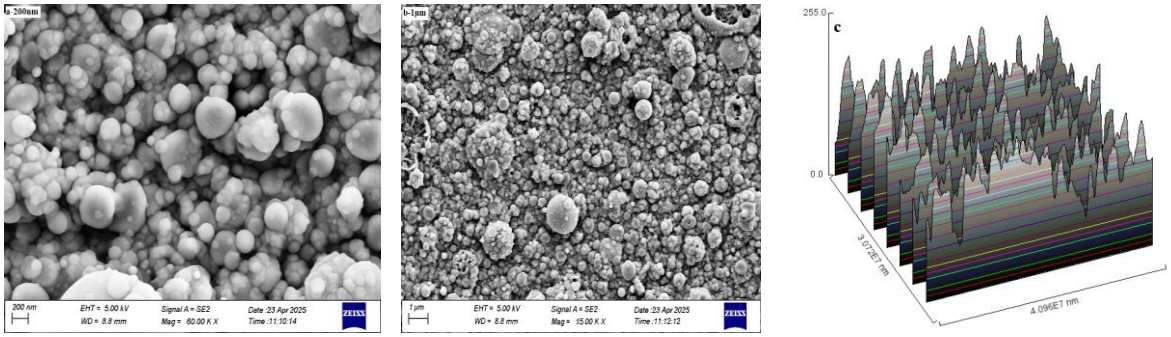

Figure 5: FE-SEM images of V_2O_5 thin film a) 200nm, b) 1µm, c) dense distribution surface.

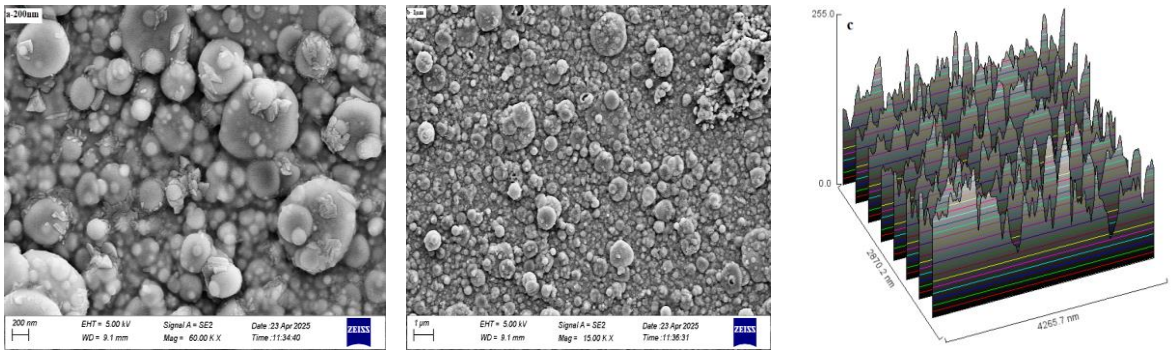

Figure 6: FE-SEM images of In_2O_3 20%- V_2O_5 80% thin film a-200nm b-1µm c-dense distribution.

Table 2: Parameters of structural properties.

Sample	2θ (degree)	D_{avg} (nm)	d_{hkl} (Å)	FWHM (degree)	hkl	Reference pattern
In_2O_3	30.58	43.58	2.917	0.189	(222)	ICSD 01-071-2194
	35.46	53.13	2.527	0.157	(400)	
	51.02	48.64	1.787	0.181	(440)	
	21.49	41.25	3.959	0.196	(211)	
V_2O_5	20.26	14.91	4.37	0.541	(001)	ICSD 00-041-1426
	12.67	14.77	6.98	0.541	(010)	ICDD 00-054-0538
	26.127	16.57	3.40	0.492	(110)	ICSD 00-041-1426
	31	16.75	2.88	0.492	(301)	
In_2O_3 20%- V_2O_5 80%	29.73	27.84	3	0.29	(222)	ICSD 01-071-2194
	35.38	21.18	2.53	0.39	(400)	
	12.59	23.209	7.02	0.34	(010)	ICDD 00-054-0538
	20.84	27.36	4.24	0.29	(001)	ICSD 00-041-1426
	26.39	27.64	3.37	0.29	(110)	
	31.05	20.94	2.87	0.39	(301)	

3.3 Optical Properties Results

Figure 7: optical transmission spectra of the thin films were recorded using a Shimadzu UV-160/UV-Visible spectrophotometer, where the films were analyzed through experimental measurements of transmittance from 350 to 1000nm the transparency of thin films for deposited by PLD shows a sharp decrease in the UV region. The transmission percentage of In_2O_3 films also varies with increasing wavelength. All samples demonstrate optical transparency in the spectral range of 500 to 900 nm. However, the transmittance reduces in the band gap region. The thin film transmittance is high at wavelengths in the visible and near-infrared regions. as the transmittance decreases when approaches the infrared (infrared) wavelengths. This is due to the indium oxide thin film is reflective at wavelengths in this region, which makes it an anti-reflective material. From Beer-Lambert law, which determines the optical absorption coefficient (α) from the transmittance[11], [25].

$$\alpha = 2.303\ A_0/t, \qquad (1)$$

where A_0 represents absorption and (t) is the thickness of the thin film In_2O_3,V_2O_5, In_2O_3-V_2O_5 280.2nm, 651nm, 301nm via cross sction respectively. The optical energy gap values of the In_2O_3 films were determined from transmission measurements by plotting $(\alpha h\nu)^2$ against (hν), as showen in Figure 8 According to the absorption spectra of the In_2O_3 films, there is a linear relationship beyond the absorption edge leading to a direct transition inference of the linear part to the x-axis provides the values for the optical band gap(3.31ev) [24].

The samples made using the PLD method at a deposition temperature of 100 °C are the source of the optical transmittance spectra shown in Figures 9 and 10. High optical transmittance is evident in the spectra, making it appropriate for the creation of photodetectors and solar cells. The samples that were not annealed after deposition showed high transmittance in the 400–700 nm range [26].

The peak at 428 nm, which shows that the films are non-homogeneous in optical transmittance behavior, is interesting to observe. According to other

research on vanadium oxide films smaller than 400 nm, we can therefore conclude that the films exist in multiphase forms. The spectrum shows a significant increase in transmittance within the 300 to 1000 nm wavelength range For the two samples shown in the Figure 9 and Figure 10, [16], [27].

Figures 11 and 12 show a clear, sharp rising edge, confirming the upward bending feature caused by charge accumulation at the interface. The optical energy gap of the films was 2.61 and 2.83 (eV) for the V_2O_5 and In_2O_3 20%-V_2O_5 80%, respectively. The optical energy gap increased significantly compared with $V_2O_5$80%. This is due to the shift of the local levels away from the conduction band resulting from the presence of 20% indium oxide [28], [29].

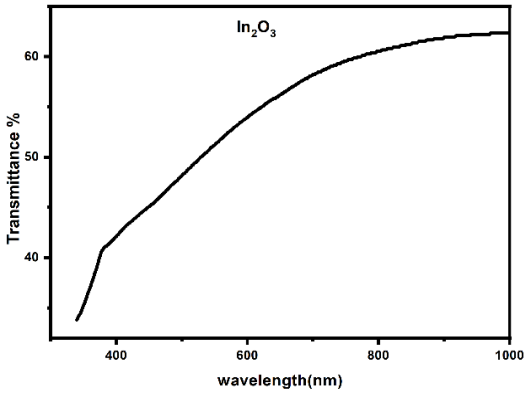

Figure 7: transmittance characteristics on the glass substrates.

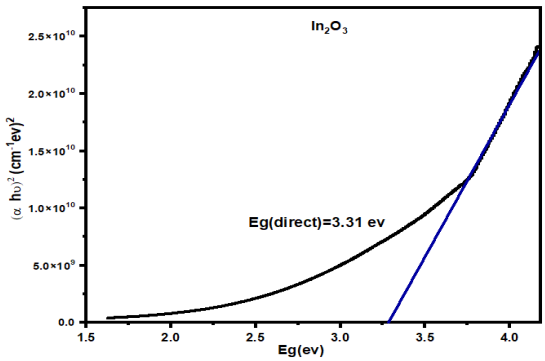

Figure 8: Energy gap for In2O3 On the glass substrates.

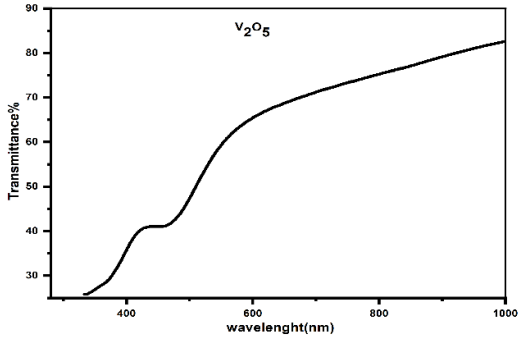

Figure 9: Transmittance of V2O5 on the glass substrates.

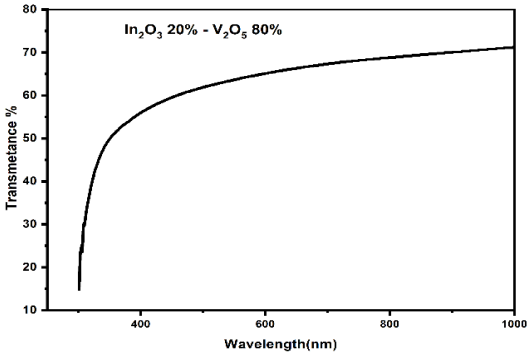

Figure 10: Transmittance of In2O3 20%- V2O5 80% the glass substrates.

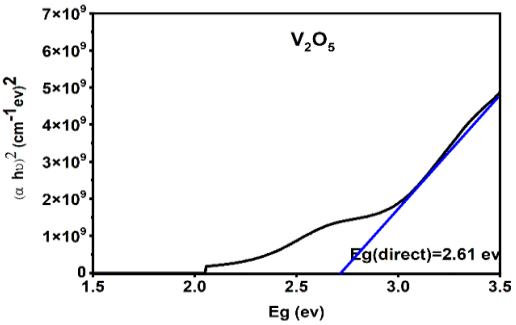

Figure 11: Energy gap for V_2O_5 on the glass substrates.

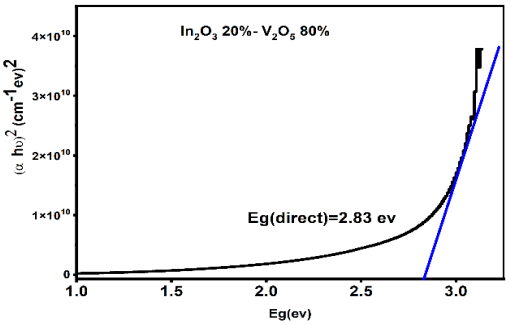

Figure 12: Energy gap for In_2O_3 20%-V_2O_5 80% on the glass substrates.

4 CONCLUSIONS

In this study, indium trioxide (In_2O_3) and vanadium pentoxide (V_2O_5) thin films were successfully synthesized by pulsed laser deposition using a 1064 nm Nd: YAG laser. The structural, morphological, and optical investigations provided the following key finding.

X-ray diffraction analysis confirmed the formation of polycrystalline In_2O_3 with a cubic bixbyite structure and orthorhombic V_2O_5 with well-defined crystallinity. The mixing ratio influenced the crystallite size. Moreover, the incorporation of V_2O_5 into the In_2O_3 matrix resulted in noticeable modifications to the structural properties, including slight peak broadening and shifts in diffraction angles, which indicate lattice distortion and the possible formation of interfacial strain. These effects suggest enhanced structural disorder at higher V_2O_5 content, while maintaining overall phase stability of the mixed system.

Field emission scanning electron microscopy (FESEM) revealed uniform, dense, and crack-free films with nanostructured surface morphology. The particle size distribution suggested that PLD-assisted growth promotes compact films suitable for optoelectronic applications.

UV–Vis absorption spectra demonstrated strong absorption edges in the visible region. The estimated optical band gaps were ~3.31–3.5 eV for In_2O_3 and ~2.61–2.68 eV for V_2O_5, consistent with reported values. These band gaps confirm the semiconducting nature of the films and their potential in transparent conducting electrodes, gas sensors, and photocatalytic devices.

The study highlights the efficiency of 1064 nm pulsed laser deposition in producing high-quality oxide thin films with controlled microstructure and desirable optical properties. Both In_2O_3 and V_2O_5 films synthesized under optimized conditions demonstrate promising potential for integration into optoelectronic and energy-related applications.

ACKNOWLEDGMENTS

The authors would like to express their sincere gratitude to the Department of Physics, College of Science, University of Diyala, for their continuous support and provision of the necessary facilities to conduct this research. The authors also extend their appreciation to all colleagues and technical staff whose guidance and assistance contributed to the successful completion of this study.

REFERENCES

[1] B. P. Yalagala, P. Sahatiya, C. S. R. Kolli, S. Khandelwal, V. Mattela, and S. Badhulika, "V2O5 nanosheets for flexible memristors and broadband photodetectors," ACS Applied Nano Materials, vol. 2, no. 2, pp. 937-947, 2019, [Online]. Available: https://doi.org/10.1021/acsanm.8b02233.

[2] Y. Vijayakumar, D. S. Jyothi, P. Nagaraju, and M. V. Reddy, "Structural, electrical and optical properties of spray deposited V2O5 thin films on glass substrates," Physica Chemica Glasses: Journal of Glass Science and Technology Part B, vol. 57, no. 1, pp. 37-41, 2016.

[3] V. Raju et al., "Superior cathode of sodium-ion batteries: orthorhombic V2O5 nanoparticles generated in nanoporous carbon by ambient hydrolysis deposition," Nano Letters, vol. 14, no. 7, pp. 4119-4124, 2014.

[4] D. Su et al., "Dimension mediated optic and catalytic performance over vanadium pentoxides," Applied Surface Science, vol. 389, pp. 112-117, 2016.

[5] Y. Zhang et al., "Dodecahedron-shaped porous vanadium oxide and carbon composite for high-rate lithium ion batteries," ACS Applied Materials & Interfaces, vol. 8, no. 27, pp. 17303-17311, 2016.

[6] Y.-L. Chan, S.-Y. Pung, and S. Sreekantan, "Synthesis of V2O5 nanoflakes on PET fiber as visible-light-driven photocatalysts for degradation of RhB dye," Journal of Catalysis, vol. 2014, no. 1, pp. 370696, 2014.

[7] Chen, "A review of emerging non-volatile memory (NVM) technologies and applications," Solid-State Electronics, vol. 125, pp. 25-38, 2016.

[8] X. Xu et al., "Vanadium-doped tin oxide porous nanofibers: Enhanced responsivity for hydrogen detection," Talanta, vol. 167, pp. 638-644, 2017, [Online]. Available: https://doi.org/10.1016/j.talanta.2017.03.013.

[9] S. Parhoodeh and M. Kowsari, "Synthesis, characterization and study of band gap variations of vanadium doped indium oxide nanoparticles," Physica B: Condensed Matter, vol. 498, pp. 27-32, 2016, [Online]. Available: https://doi.org/10.1016/j.physb.2016.06.020.

[10] Y.-C. Lin, J.-H. Lin, and R.-Y. Hsu, "Vanadium-doped indium tin oxide window layer in Sb2Se3 solar cell," Journal of Physics and Chemistry of Solids, vol. 165, pp. 110661, 2022, [Online]. Available: https://doi.org/10.1016/j.jpcs.2022.110661.

[11] P. Prathap et al., "Anti-reflection In2O3 nanocones for silicon solar cells," Solar Energy, 2014, [Online]. Available: https://doi.org/10.1016/j.solener.2013.12.037.

[12] R. T. R. Kumar, B. Karunagaran, V. S. Kumar, Y. L. Jeyachandran, D. Mangalaraj, and S. K. Narayandass, "Structural properties of V2O5 thin films prepared by vacuum evaporation," Materials Science in Semiconductor Processing, vol. 6, no. 5-6, pp. 543-546, 2003.

[13] H. Fu, "Synthesis of vanadium oxide nanostructures for functional applications", 2013, [Online]. Available: https://doi.org/10.1016/j.tsf.2007.08.113.

[14] P. Zibrov, V. P. Filonenko, S. G. Lyapin, and V. A. Sidorov, "The high pressure phases β- and δ-V2O5: Structure refinement, electrical and optical properties, thermal stability," High Pressure Research, vol. 33, no. 2, pp. 399-408, 2013, [Online]. Available: https://doi.org/10.1080/08957959.2013.796375.

[15] V. P. Filonenko, M. Sundberg, P. E. Werner, and I. P. Zibrov, "Structure of a high-pressure phase of vanadium pentoxide, β-V2O5," Acta Crystallographica Section B: Structural Science, vol. 60, no. 4, pp. 375-381, 2004, [Online]. Available: https://doi.org/10.1107/S0108768104012881.

[16] S. Beke, S. Giorgio, L. Korösi, L. Nánai, and W. Marine, "Structural and optical properties of pulsed laser deposited V2O5 thin films," Thin Solid Films, vol. 516, no. 15, pp. 4659-4664, 2008, [Online]. Available: https://doi.org/10.1016/j.tsf.2007.08.113.

[17] H. Shah, Y. Liu, V. T. Nguyen, G. S. Zakharova, I. Mehmood, and W. Chen, "Enhanced ultra-stable n-propylamine sensing behavior of V2O5/In2O3 core-shell nanorods," RSC Advances, vol. 5, no. 67, pp. 54412-54419, 2015, [Online]. Available: https://doi.org/10.1039/c5ra06531c.

[18] M. G. Kim et al., "Synthesis of V-doped In2O3 nanocrystals via digestive-ripening process and their electrocatalytic properties in CO2 reduction reaction," ACS Applied Materials & Interfaces, vol. 12, no. 10, pp. 11890-11897, 2020, [Online]. Available: https://doi.org/10.1021/acsami.9b19584.

[19] El Hichou, M. Addou, M. Mansori, and J. Ebothé, "Structural, optical and luminescent characteristics of sprayed fluorine-doped In2O3 thin films for solar cells," Solar Energy Materials and Solar Cells, vol. 93, no. 5, pp. 609-612, 2009, [Online]. Available: https://doi.org/10.1016/j.solmat.2008.12.014.

[20] Y. Liu et al., "Solution processed W-doped In2O3 thin films with high carrier mobility," Ceramics International, vol. 46, no. 2, pp. 2173-2177, 2020, [Online]. Available: https://doi.org/10.1016/j.ceramint.2019.09.201.

[21] D. R. T. Alrayyes, M. A. Fakhri, A. A. Alwahib, M. A. Qaeed, and S. C. B. Gopinath, "Physical investigations of In2O3/porous silicon at different laser wavelengths," International Journal of Nanoelectronics and Materials, vol. 17, pp. 69-76, 2024, [Online]. Available: https://doi.org/10.58915/ijneam.v17iJune.837.

[22] Y. Deng, A. Pelton, and R. A. Mayanovic, "Comparison of vanadium oxide thin films prepared using femtosecond and nanosecond pulsed laser deposition," MRS Advances, vol. 1, no. 39, pp. 2737-2742, 2016.

[23] O. Voloshyna, M. V. Gorbunov, D. Mikhailova, A. Maljuk, S. Seiro, and B. Büchner, "Flux growth and characterization of bulk InVO4 crystals," Crystals, vol. 13, no. 10, 2023, [Online]. Available: https://doi.org/10.3390/cryst13101439.

[24] C. V. Ramana, R. J. Smith, O. M. Hussain, C. C. Chusuei, and C. M. Julien, "Correlation between growth conditions, microstructure, and optical properties in pulsed-laser-deposited V2O5 thin films," pp. 1213-1219, 2005.

[25] M. Ali, "Energy band diagram of In2O3/Si heterojunction," Baghdad Science Journal, vol. 8, no. 2, pp. 21, 2011.

[26] E. A. A. Arbab and G. T. Mola, "V2O5 thin film deposition for application in organic solar cells," Applied Physics A: Materials Science & Processing, vol. 122, no. 4, 2016, [Online]. Available: https://doi.org/10.1007/s00339-016-9966-1.

[27] Y. Iida, Y. Kaneko, and Y. Kanno, "Fabrication of pulsed-laser deposited V2O5 thin films for electrochromic devices," Journal of Materials Processing Technology, vol. 197, no. 1-3, pp. 261-267, 2008, [Online]. Available: https://doi.org/10.1016/j.jmatprotec.2007.06.032.

[28] R. Van de Krol, J. Ségalini, and C. S. Enache, "Influence of point defects on the performance of InVO4 photoanodes," vol. 7770, pp. 77700S, 2010, [Online]. Available: https://doi.org/10.1117/12.860463.

[29] R. Irani, S. M. Rozati, and S. Beke, "Effects of the precursor concentration and different annealing ambients on the structural, optical, and electrical properties of nanostructured V2O5 thin films deposited by spray pyrolysis technique," Applied Physics A: Materials Science & Processing, vol. 124, no. 4, pp. 0, 2018, [Online]. Available: https://doi.org/10.1007/s00339-018-1744-9.